



## Photogenerated Radical in Phenylglyoxylic Acid for in Vivo Hyperpolarized $^{13}\text{C}$ MR with Photosensitive Metabolic Substrates

Marco-Rius, Irene; Cheng, Tian; Gaunt, Adam P.; Patel, Saket; Kreis, Felix; Capozzi, Andrea; Wright, Alan J.; Brindle, Kevin M.; Ouari, Olivier; Comment, Arnaud

*Published in:*  
Journal of the American Chemical Society

*Link to article, DOI:*  
[10.1021/jacs.8b09326](https://doi.org/10.1021/jacs.8b09326)

*Publication date:*  
2018

*Document Version*  
Peer reviewed version

[Link back to DTU Orbit](#)

*Citation (APA):*  
Marco-Rius, I., Cheng, T., Gaunt, A. P., Patel, S., Kreis, F., Capozzi, A., Wright, A. J., Brindle, K. M., Ouari, O., & Comment, A. (2018). Photogenerated Radical in Phenylglyoxylic Acid for in Vivo Hyperpolarized  $^{13}\text{C}$  MR with Photosensitive Metabolic Substrates. *Journal of the American Chemical Society*.  
<https://doi.org/10.1021/jacs.8b09326>

---

### General rights

Copyright and moral rights for the publications made accessible in the public portal are retained by the authors and/or other copyright owners and it is a condition of accessing publications that users recognise and abide by the legal requirements associated with these rights.

- Users may download and print one copy of any publication from the public portal for the purpose of private study or research.
- You may not further distribute the material or use it for any profit-making activity or commercial gain
- You may freely distribute the URL identifying the publication in the public portal

If you believe that this document breaches copyright please contact us providing details, and we will remove access to the work immediately and investigate your claim.

Article

# Photo-generated radical in phenylglyoxylic acid for in vivo hyperpolarized C-MR with photo-sensitive metabolic substrates

Irene Marco-Rius, Tian Cheng, Adam P. Gaunt, Saket Patel, Felix Kreis, Andrea Capozzi, Alan Wright, Kevin M. Brindle, Olivier Ouari, and Arnaud Comment

*J. Am. Chem. Soc.*, **Just Accepted Manuscript** • DOI: 10.1021/jacs.8b09326 • Publication Date (Web): 12 Oct 2018

Downloaded from <http://pubs.acs.org> on October 15, 2018

## Just Accepted

"Just Accepted" manuscripts have been peer-reviewed and accepted for publication. They are posted online prior to technical editing, formatting for publication and author proofing. The American Chemical Society provides "Just Accepted" as a service to the research community to expedite the dissemination of scientific material as soon as possible after acceptance. "Just Accepted" manuscripts appear in full in PDF format accompanied by an HTML abstract. "Just Accepted" manuscripts have been fully peer reviewed, but should not be considered the official version of record. They are citable by the Digital Object Identifier (DOI®). "Just Accepted" is an optional service offered to authors. Therefore, the "Just Accepted" Web site may not include all articles that will be published in the journal. After a manuscript is technically edited and formatted, it will be removed from the "Just Accepted" Web site and published as an ASAP article. Note that technical editing may introduce minor changes to the manuscript text and/or graphics which could affect content, and all legal disclaimers and ethical guidelines that apply to the journal pertain. ACS cannot be held responsible for errors or consequences arising from the use of information contained in these "Just Accepted" manuscripts.



ACS Publications

is published by the American Chemical Society, 1155 Sixteenth Street N.W., Washington, DC 20036

Published by American Chemical Society. Copyright © American Chemical Society. However, no copyright claim is made to original U.S. Government works, or works produced by employees of any Commonwealth realm Crown government in the course of their duties.

# Photo-generated radical in phenylglyoxylic acid for in vivo hyperpolarized $^{13}\text{C}$ MR with photo-sensitive metabolic substrates

Irene Marco-Rius,<sup>a\*</sup> Tian Cheng,<sup>a</sup> Adam P. Gaunt,<sup>a</sup> Saket Patel,<sup>b</sup> Felix Kreis,<sup>a</sup> Andrea Capozzi,<sup>c</sup> Alan J. Wright,<sup>a</sup> Kevin M. Brindle,<sup>a</sup> Olivier Ouari,<sup>b</sup> and Arnaud Comment<sup>a,d</sup>

<sup>a</sup> University of Cambridge, Cambridge, UK ; <sup>b</sup> Aix-Marseille University, CNRS, ICR, Marseille, France ; <sup>c</sup> Department of Electrical Engineering, Center for Hyperpolarization in Magnetic Resonance, Technical University of Denmark, Lyngby, Denmark; <sup>d</sup> General Electric Healthcare, Chalfont St Giles, UK.

*Photolysis; Dynamic Nuclear Polarization; Hyperpolarization; Benzoylformic acid; Dihydroxyacetone*

**ABSTRACT:** Whether for  $^{13}\text{C}$  magnetic resonance studies in chemistry, biochemistry or biomedicine, hyperpolarization methods based on dynamic nuclear polarization (DNP) have become ubiquitous. DNP requires a source of unpaired electrons, which are commonly added to the sample to be hyperpolarized in the form of stable free radicals. Once polarized, the presence of these radicals is unwanted. These radicals can be replaced by non-persistent radicals created by photo-irradiation of pyruvic acid (PA), which are annihilated upon dissolution or thermalization in the solid state. However, since PA is readily metabolized by most cells, its presence may be undesirable for some metabolic studies. In addition, some  $^{13}\text{C}$  substrates are photo-sensitive and, therefore, may degrade during photo-generation of PA radical, which requires ultraviolet (UV) light. We show here that photo-irradiation of phenylglyoxylic acid (PhGA) using visible light produces a non-persistent radical that, in principle, can be used to hyperpolarize any molecule. We compare radical yields in samples containing PA and PhGA upon photo-irradiation with broadband and narrowband UV-visible light sources. To demonstrate the suitability of PhGA as a radical precursor for DNP, we polarized the gluconeogenic probe  $^{13}\text{C}$ -dihydroxyacetone, which is UV-sensitive, using a commercial 3.35 T DNP polarizer and then injected this into a mouse and followed its metabolism in vivo.

## INTRODUCTION

Hyperpolarization by dissolution dynamic nuclear polarization (DNP) can enhance the magnetic resonance (MR) signals of molecules in solution by up to 5 orders of magnitude.<sup>1</sup> As the list of molecules that have been hyperpolarized increases every year, so do applications across organic and polymer chemistry,<sup>2</sup> as well as biomedicine.<sup>3</sup> DNP is based on transfer of spin polarization from unpaired electrons of stable free radicals to nuclei at cryogenic temperatures. Stable radicals such as trityls, nitroxides or 1,3-bisdiphenylene-2-phenylallyl (BDPA) are admixed with the sample containing the molecule to be hyperpolarized.<sup>4</sup> A consequence of having to introduce stable radicals is that they accelerate nuclear spin relaxation, which may cause significant signal loss during the dissolution process. A concern for applications in the biomedical field, where dissolution DNP has seen a rapid translation from the laboratory to the clinic,<sup>5–7</sup> is the potential radical toxicity. Medical regulatory bodies currently demand that radicals are filtered out prior to injection into a human subject,<sup>8,9</sup> which adds to the complexity of the process and becomes a potential failure point before the release of the solution for injection.

Non-persistent photo-induced free radicals generated by ultraviolet (UV) light irradiation of pyruvic acid (PA) have been proposed as an alternative to the persistent radicals used in dissolution DNP.<sup>10</sup> Recently it has been demonstrated that these non-persistent radicals can be annihilated inside the frozen sample by warming it to  $\sim 200$  K. After this point, the nuclear spin hyperpolarization can persist for several hours,<sup>11</sup> making it possible to transport the sample for use at a distant location. Several  $^{13}\text{C}$ -labeled metabolic substrates have

been hyperpolarized using PA as a precursor molecule for photo-generation of radicals.<sup>12,13</sup> However, when PA itself is not one of the substrates of interest,<sup>10,13</sup> metabolic interference caused by its presence may be undesirable. Furthermore, PA cannot be considered a universal polarizing agent because some metabolic substrates are photo-sensitive and can degrade during the exposure to UV light when generating the radical. One example of this problem is  $[2-^{13}\text{C}]$ dihydroxyacetone (DHAc), which has been previously hyperpolarized with OX063 trityl radical and used to study gluconeogenesis, glycolysis and fatty acid synthesis in the liver<sup>14–16</sup>. DHAc absorbs light below 300 nm leading to sample degradation.<sup>17</sup> Finally, dimethyl sulfoxide (DMSO), which is frequently used as glassing agent for the preparation of DNP samples, is also photo-sensitive.

The purpose of this work is to demonstrate that phenylglyoxylic acid (PhGA) can also be used as an efficient radical precursor for DNP. PhGA has an excellent safety profile and no reported effect on metabolism on the timescale of the hyperpolarized  $^{13}\text{C}$  MR experiments.<sup>18</sup> Because of its extended absorption into the visible spectrum, a radical can be photo-generated in PhGA at longer wavelengths and can therefore be used in conjunction with molecules that are sensitive to UV light. We show that  $[2-^{13}\text{C}]$ DHAc can be hyperpolarized using the photo-generated radical of PhGA and a commercial 3.35 T HyperSense polarizer, and that the resulting solution can be used for  $^{13}\text{C}$  MR metabolic studies in vivo.

## EXPERIMENTAL SECTION

All chemicals were purchased from Sigma-Aldrich (Haverhill, UK) and data were processed in MATLAB (Mathworks, Natick, MA, USA), unless stated otherwise.

## UV-Vis absorption measurements

The ultraviolet–visible (UV-Vis) absorption spectra of PhGA, PA, DHAc and DMSO in water (146 mM, 600  $\mu$ l) were measured using an Ocean Optics USB2000+ spectrometer and DH-2000-BAL UV-VIS-NIR light source (Halma PLC, Amersham, UK).

To estimate the efficiency of broadband and narrowband UV-Vis light sources in generating photo-induced radicals in PA and PhGA, the power profile of each source (provided by the manufacturer) was multiplied by the absorption spectrum of PA and PhGA between 300 nm and 420 nm (Fig. 1). The integral of the multiplied spectra was used to compare the effective light intensity provided by each source.

## Broadband and narrowband photo-irradiation

To investigate the effects of photo-irradiation on the selected radical precursors, two solutions were prepared: neat PA diluted to 7.0 M in a mixture of 1:1 glycerol/water (v/v) and sonicated for 5 min at 40  $^{\circ}$ C; and a sample containing 7.1 M PhGA in a mixture of 1:1 glycerol/water (v/v) sonicated for 5 min at 40  $^{\circ}$ C. To study the relationship between PhGA concentration, light source and radical yield, the 7.1 M PhGA sample was diluted to 50%, 25% and 7% of the original PhGA concentration in a mixture of 1:1 glycerol/water (v/v). Additionally, the effect of the light sources on two photo-sensitive solutions was tested: neat dimethyl sulfoxide (DMSO); and a sample containing 8.0 M DHAc dissolved in  $^2$ H $_2$ O sonicated for 10 min at 40  $^{\circ}$ C.

Frozen beads of each solution were formed by dispensing droplets from a syringe into an ESR quartz dewar flask (Wilma-Lab Glass WG-850-B-Q, Goss Scientific, Crewe, UK) filled with liquid nitrogen (LN $_2$ ). The beads were photo-irradiated using either a broadband source (Dymax BlueWave 75, Dymax Europe GmbH, Wiesbaden, Germany) or a narrowband source (Dymax BlueWave LED VisiCure 405 nm, Dymax Europe GmbH, Wiesbaden, Germany) operating at maximum power. From this point onwards these two sources are referred to as “BlueWave 75” and “VisiCure 405”. The stand used for UV irradiation is described in ref. <sup>19</sup>. Note that transmission through the quartz dewar was the same across the entire range of wavelengths used in this study.<sup>20</sup>

## X-band ESR measurements and radical concentration estimation

ESR spectra of single frozen beads inside the quartz dewar filled with LN $_2$  were acquired using a benchtop X-band ESR spectrometer (MiniScope MSS000, Magnetech GmbH, Berlin, Germany). ESR parameters were optimized to resolve the hyperfine structure of the spectra and then kept constant throughout all the experiments (number of accumulations = 1, B = [323–353] mT, sweep time = 20 s, modulation amplitude = 0.1 mT, modulation frequency = 100 kHz, microwave power = 0.2 mW). Sequential ESR spectra were acquired for each bead after different irradiation times to obtain a radical build-up curve (Sup. Fig. 2). The effect of deuterating PhGA on the ESR line width was investigated by substituting protonated PhGA in water with perdeuterated PhGA (d $_5$ -PhGA) in  $^2$ H $_2$ O. The synthesis of d $_5$ -PhGA is detailed in the Supporting Information.

Following ESR signal acquisition, the frozen bead was extracted from the quartz dewar, inserted into an Eppendorf tube and weighed to estimate the volume of the bead. Radical concentration was determined by comparing double integration of the first derivative ESR spectrum, corrected for bead volume ( $\sim$ 4  $\mu$ l), with a calibration curve obtained from beads of known concentrations of 4-Hydroxy-2,2,6,6-tetramethylpiperidine 1-oxyl (TEMPOL, Sup. Fig. 1). Each measurement was repeated at least twice.

## Dynamic nuclear polarization

Four samples were prepared for dissolution DNP: (sample #1) 8 M [2- $^{13}$ C]DHAc and 1 M PhGA in water; (sample #2) 8 M [2- $^{13}$ C]DHAc, 1 M PhGA and 1.2 mM gadoteric acid (Gd $^{3+}$ , Dotarem, Guerbet, Roissy, France) in water; (sample #3) 8 M [2- $^{13}$ C]DHAc, 1 M d $_5$ -PhGA and 1.2 mM Gd $^{3+}$  in  $^2$ H $_2$ O; and (sample #4) 8 M [2- $^{13}$ C]DHAc, 21 mM OX063 trityl radical (Albeda Research Aps, Copenhagen, Denmark) and 1.2 mM Gd $^{3+}$  in 1:3 DMSO/water (v/v). All solutions were sonicated for 5 min at 50  $^{\circ}$ C before addition of Gd $^{3+}$ . The choice of PhGA concentration in samples #1, #2 and #3 was based on the fact that hyperpolarized DHAc had previously been polarized with 21 mM OX063,<sup>14–16</sup> a radical with a similar ESR line width as the one obtained after photo-irradiation of PhGA, and that a similar concentration of photo-generated radical (18–20 mM) can be obtained if the samples are doped with 1 M PhGA.

Between 7 and 11 beads of samples #1, #2 and #3 were simultaneously irradiated for 200 s with the VisiCure 405 source. The beads were then placed into a standard HyperSense sample holder in contact with LN $_2$  to preserve the radical and rapidly inserted into a HyperSense polarizer operating at 3.35 T and 1.25 K (Oxford Instruments, Abingdon, UK). A microwave ( $\mu$ -wave) sweep between 94.07 GHz and 94.22 GHz (10 MHz steps, 10-min  $\mu$ -wave irradiation/step) was performed for samples #2, #3 and #4 and for a sample containing 7 M [1- $^{13}$ C]PA in 1:1 glycerol/water (v/v) irradiated for 400 s with the BlueWave 75 source. The background signal measured at each  $\mu$ -wave frequency was subtracted from all  $\mu$ -wave sweeps. For dissolution DNP, samples were polarized with the  $\mu$ -wave source set to 94.110 GHz (except the sample used for the in vivo experiment, which was polarized at 94.205 GHz) and 100 mW for a period of 1.5–2 h. The samples were dissolved with 6 ml of a phosphate saline buffer (PBS).

## Hyperpolarized $^{13}$ C MR in a phantom at 7 T

Liquid-state  $^{13}$ C MR acquisitions were carried out in a small-animal horizontal bore 7 T MR scanner (Agilent, Palo Alto, CA) using a 42-mm-diameter bird-cage  $^1$ H/ $^{13}$ C transmit volume coil and a 20 mm outer diameter  $^{13}$ C receive surface coil (Rapid Biomedical GmbH, Rimpf, Germany). The temporal evolution of the hyperpolarized  $^{13}$ C signal was recorded in a 3 mL phantom starting  $16 \pm 1$  s after dissolution using the following parameters: repetition time = 1 s, nominal flip angle = 9  $^{\circ}$ , pulse width = 400  $\mu$ s (sinc pulse truncated to 5 lobes), spectral width = 32 kHz. T $_1$  relaxation time constants were determined by fitting an exponential decay function to the data and corrected for the flip angle (see Suppl. Inf. for details on the mathematical formula).

The thermal equilibrium  $^{13}$ C MR signal was acquired with the same parameters but a longer repetition time ( $\sim$ 5 $\times$ T $_1$ ) and the  $^{13}$ C hyperpolarization at the time of the first acquisition was calculated as the ratio between the hyperpolarized and thermal signals multiplied by the theoretical equilibrium polarization at 7 T and 298 K.

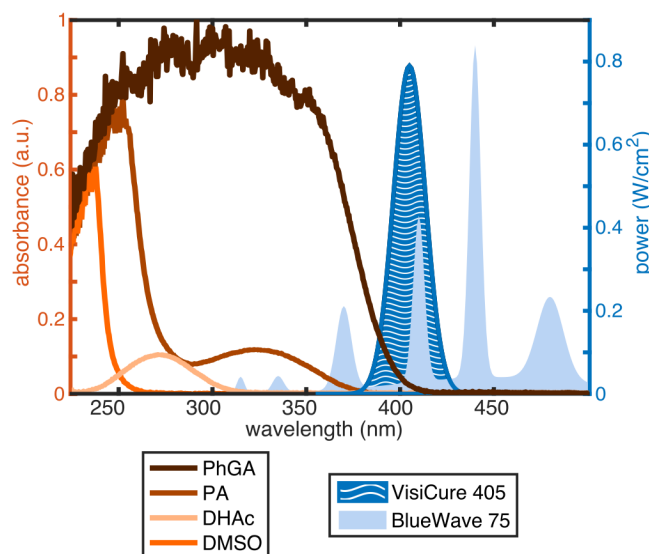


Figure 1. UV-Vis absorption spectra (left axis) and light source power distributions (right axis). Power profiles were provided by the manufacturer (Dymax Europe GmbH, Wiesbaden, Germany).

**Table 1. Maximum radical yield after photo-irradiation**

Precursor	Radical yield (mM) BlueWave 75	Radical yield (mM) VisiCure 405
PhGA (7.1M)	25.7 ± 3.7	40.4 ± 5.8
PA (7.0M)	77.7 ± 11.2	23.8 ± 3.4

### In vivo hyperpolarized $^{13}\text{C}$ MR at 7T

Procedures were performed in compliance with project and personal licenses issued under the United Kingdom Animals (Scientific Procedures) Act, 1986 and were approved by the Cancer Research UK, Cambridge Institute Animal Welfare and Ethical Review Body. A female C57B6 mouse (body weight = 32.2 g) was anesthetized with 2% isoflurane, its body temperature maintained at 37°C, and placed inside the 7 T MR system. The coil setup was identical to the one used for the phantom experiments (a 42-mm-diameter bird-cage  $^1\text{H}/^{13}\text{C}$  transmit volume coil and a 20 mm outer diameter  $^{13}\text{C}$  receive surface coil; Rapid Biomedical GMBH, Rimpar, Germany), with the receive surface coil placed over the liver of the mouse. Positioning of the surface coil was confirmed with sagittal, coronal and axial  $T_2$ -weighted  $^1\text{H}$  images.

Photo-irradiated beads ( $\sim 30\ \mu\text{l}$ ) from sample #2 were polarized as described above with  $\mu$ -wave irradiation at 94.205 GHz and dissolved in 6 ml of PBS. 400  $\mu\text{l}$  of this solution was injected into the mouse via a tail-vein over a period of 3 s.  $^{13}\text{C}$  MR acquisition started 12 s after the injection. The parameters used for  $^{13}\text{C}$  MR acquisition were: repetition time = 0.2 s, nominal flip angle = 15°, pulse width = 2 ms (sinc pulse truncated to 5 lobes), spectral width = 6 kHz, total acquisition time = 80 s. The transmitter was centered at 72.3 ppm, and every 10<sup>th</sup> acquisition it was switched to 214 ppm for a single acquisition before returning to 72.3 ppm. Therefore, the spectral region around 72.3 ppm was sampled 360 times (every 0.2 s) and the region around 214 ppm was sampled 40 times (every 2 s). This high temporal resolution acquisition strategy was chosen to maximize the signal-to-noise ratio of the summed spectra assuming an in vivo  $T_1$  of 10 s for the metabolites (see analysis presented in ref. <sup>21</sup>). A similar scheme has previously been used for the detection of glucose metabolism in vivo.<sup>22,23</sup> The volume coil excited the whole body, and reception was coil-selective.

### Liquid-state $^{13}\text{C}$ MR at 14.1 T

Following the hyperpolarized  $^{13}\text{C}$  phantom experiments, the samples obtained after dissolution were mixed with 10%  $^2\text{H}_2\text{O}$  and their thermally-polarized  $^{13}\text{C}$  MR spectrum was measured in a 600 MHz vertical-bore Bruker spectrometer (Bruker BioSpin GmbH, Rheinstetten, Germany). To further investigate the impact of photo-irradiation on the solutions containing PhGA, the  $^{13}\text{C}$  spectra of two additional samples prepared by dissolving either a non-irradiated bead or a 200-s-irradiated bead (using VisiCure 405) in 600  $\mu\text{l}$  PBS (10%  $^2\text{H}_2\text{O}$ ) were recorded for comparison. All four samples were measured with the following parameters: repetition time = 6 s, nominal flip angle = 30°, pulse width = 2.6  $\mu\text{s}$  (hard pulse), spectral width = 38 kHz.  $T_1$ s were measured using an inversion recovery sequence.

## RESULTS

### UV-Vis absorption and light source power profiles

The UV-Vis spectra of the two precursors studied here show that PhGA has a broad absorption between 200 and 400 nm, while PA has a weaker and narrower absorption around  $\lambda_{\text{max}} = 320\ \text{nm}$  corresponding to the  $n\text{-}\pi^*$  electronic transition characteristic of  $\alpha$ -ketoacids.<sup>24</sup> The metabolic substrate DHAc has an absorption peak around  $\lambda_{\text{max}} = 270\ \text{nm}$  and the DMSO solvent one around  $\lambda_{\text{max}} = 240\ \text{nm}$  (Fig. 1).

The power dependence of the two light sources on wavelength was obtained from the manufacturer's manual and is overlaid on Figure 1. While the total output power density was nearly the same for both light sources (19 W/cm<sup>2</sup> for the BlueWave 75 and 16.8 W/cm<sup>2</sup> for the VisiCure 405), the power distribution across the spectrum was radically different. Based on the multiplied spectra calculated from the UV-Vis absorption of PA and PhGA and the wavelength-dependent power distribution of each light source, the BlueWave 75 light source was expected to be more effective for radical generation in PA while the VisiCure 405 source should be better suited for radical generation in PhGA since the ratio  $\text{Area}_{\text{broadband}} / \text{Area}_{405\text{nm}}$  is much larger for PA than for PhGA (15 vs. 2.8).

### Broadband and narrowband photo-irradiation

PhGA and PA were irradiated with either the BlueWave 75 broadband light source or the VisiCure 405 narrowband light source. The associated ESR spectra are displayed in Figures 2a and 2b. The scheme of the photochemical pathway for radical production in PhGA and PA at 77 K is shown in the Supplementary Information. Frozen PA and PhGA beads turned a yellow-orange color after irradiation, which became darker as irradiation time increased (Fig. 3a).

Table 1 summarizes the radical yield for each precursor and light source. BlueWave 75 yielded 3.3 times more radical and 3 times faster than VisiCure 405 when PA was the precursor. Conversely, irradiation of PhGA with VisiCure 405 resulted in a 1.6-fold increase in radical yield compared to broadband irradiation, without a reduction in the build-up time. The radical yield increased with PhGA concentration (Fig. 3c). It is noticeable that irradiation with either BlueWave 75 or the narrowband light source produced similar radical yields in solutions with PhGA concentrations below 1.77 M. However, irradiation with BlueWave 75 generated lower radical yields at higher PhGA concentrations.

The ESR line width of PhGA was about 3 times narrower than that of PA. Perdeuteration of PhGA ( $d_5$ -PhGA) resulted in a  $\sim 10\%$  narrower ESR line width than protonated PhGA (FWHM =  $1.30 \pm 0.05\ \text{mT}$  vs FWHM =  $1.45 \pm 0.05\ \text{mT}$ , Fig. 3b) but did not change the radical yield.

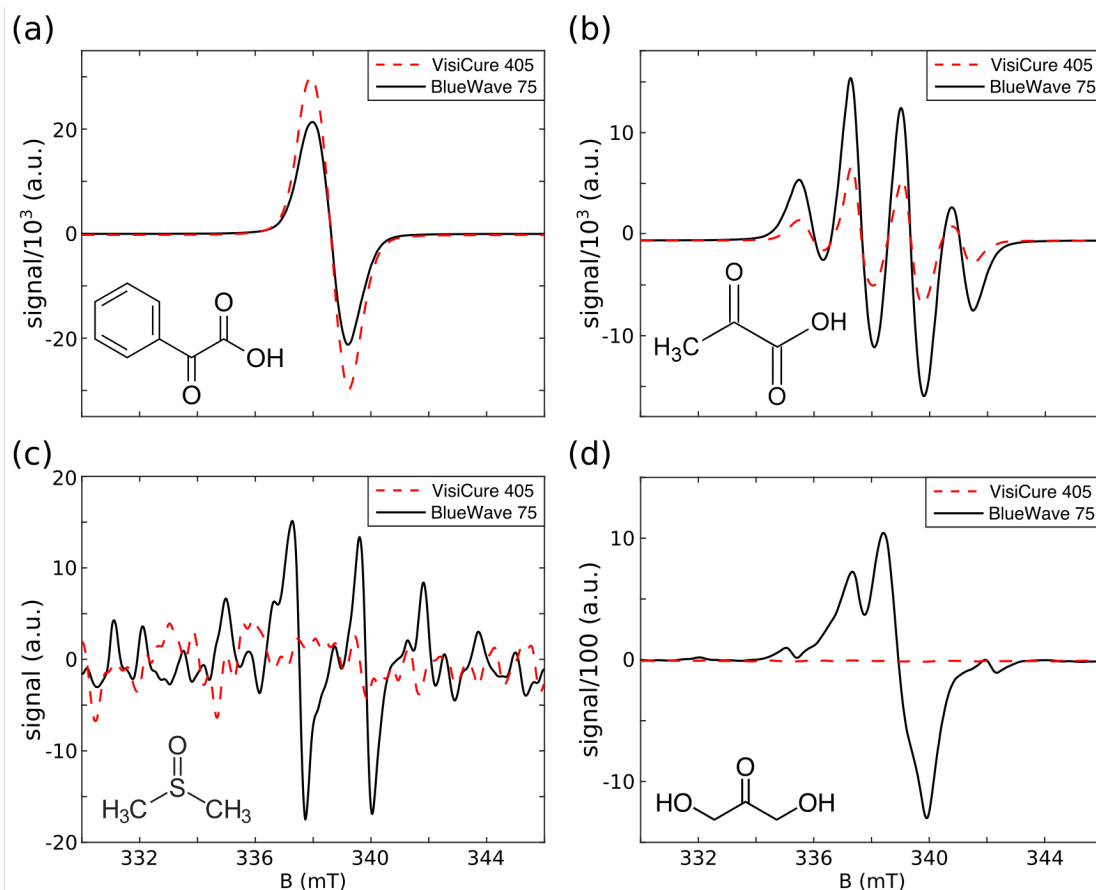


Figure 2. X-band ESR spectra of frozen droplets in  $\text{LN}_2$ , photo-irradiated with a broadband (BlueWave 75) or a narrowband (VisiCure 405) light source. (a) PhGA (7.1 M) in 1:1 water/glycerol (v/v). (b) PA (7.0 M) in 1:1 water/glycerol (v/v). (c) DMSO (neat). (d) DHAc (8.0 M) in  $^2\text{H}_2\text{O}$ . The spectral structure in (b) and (c) are caused by the hyperfine coupling to the proton spins of the methyl groups. The units on the y-axis are the same in all four plots.

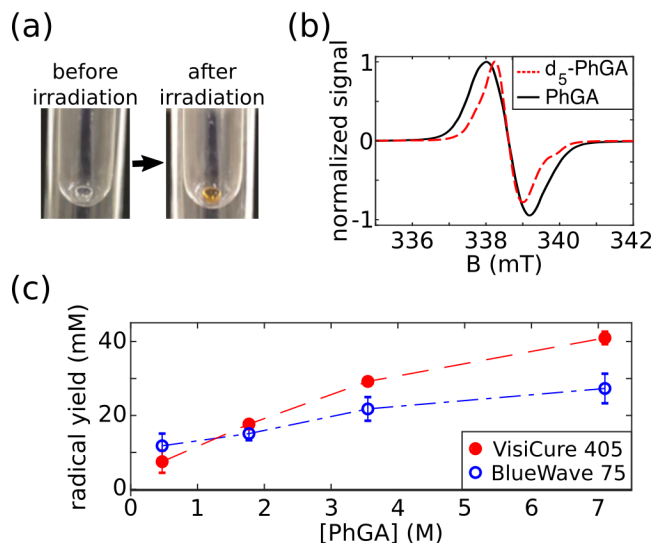


Figure 3. Photo-irradiation of PhGA dissolved in 1:1 glycerol/water (v/v). (a) 4- $\mu\text{l}$ -bead of PhGA in  $\text{LN}_2$  before and after photo-irradiation. (b) ESR spectrum of unlabeled PhGA and  $d_5$ -PhGA. (c) Maximum radical yield vs. PhGA concentration using either the broadband (blue open circle) or the narrowband light source (red dots). Radical yield is reported as mean  $\pm$  standard deviation across 3 measurements.

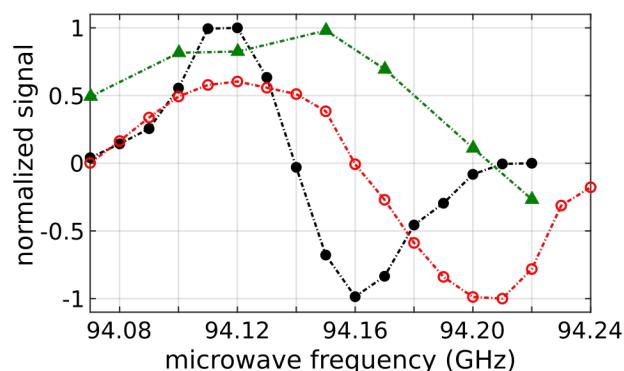


Figure 4. Solid-state microwave spectra at 3.35 T and 1.25 K: (open red circles) photo-irradiated  $[2-^{13}\text{C}]$ DHAc solution (8 M) in  $\text{H}_2\text{O}$  doped with 1 M PhGA (18 mM radical); (black dots)  $[2-^{13}\text{C}]$ DHAc solution (8 M) in  $\text{H}_2\text{O}/\text{DMSO}$  (v/v) doped with 21 mM OX063; (green triangles) photo-irradiated  $[1-^{13}\text{C}]$ PA solution (7 M) in  $\text{H}_2\text{O}/\text{glycerol}$  (65 mM radical).

The photo-sensitive metabolite DHAc and glassing agent DMSO were also irradiated with both light sources. Irradiation of DMSO and DHAc with BlueWave 75 produced radicals that were clearly observed in the ESR spectra, while irradiation with VisiCure 405 did not generate any observable radical (Fig. 2c and Fig. 2d).



### DNP of [2-<sup>13</sup>C]DHAc with PhGA-derived radical

The samples containing 8 M [2-<sup>13</sup>C]DHAc and 1 M PhGA (or d<sub>5</sub>-PhGA) in water were strongly acidic (pH = 0.5 ± 0.5). A 200-s irradiation with VisiCure 405 was sufficient to reach a plateau in radical production with a yield of 18.1 ± 2.5 mM in the samples with and without Gd<sup>3+</sup> (the variability of 5 measurements was ± 0.5 mM). No ESR signal originating from photo-irradiation of a 1 mM solution of Gd<sup>3+</sup> in water could be detected (data not shown).

The width of the μ-wave spectrum of samples containing radical generated by photolysis of PhGA was noticeably broader than the spectrum of the PA sample containing OX063 trityl radical but narrower than that for photo-irradiated PA (Fig. 4). However, unlike OX063, the μ-wave spectrum of the PhGA-derived radical was strongly asymmetric, with approximately 1.7 times higher <sup>13</sup>C polarization when the μ-wave frequency is set to the value corresponding to the optimal negative polarization, namely 94.205 ± 0.005 GHz. The build-up rate was however identical for both the negative and positive optimal frequencies and there was no noticeable difference when unlabeled PhGA was replaced by d<sub>5</sub>-PhGA (Sup. Fig. 3).

### Hyperpolarized [2-<sup>13</sup>C]DHAc

The build-up time constants as well as the liquid-state <sup>13</sup>C polarization were measured for all the [2-<sup>13</sup>C]DHAc samples (Table 2). The build-up time constant in samples containing PhGA was not affected by the addition of Gd<sup>3+</sup> or perdeuteration of PhGA. However, the liquid-state polarization increased by 1.7-fold upon addition of 1.2 mM Gd<sup>3+</sup>. The polarization values shown in Table 2 were measured approximately 16 s after the start of the dissolution process, which means that the estimated <sup>13</sup>C polarization at the time of dissolution was ~8 % for the samples doped with Gd<sup>3+</sup> and polarized with the μ-wave frequency set to 94.110 GHz. Based on the solid-state data, the <sup>13</sup>C polarization at the time of dissolution should reach ~14 % if this sample was negatively polarized at 94.205 GHz.

After dissolution, the pH was neutral in all cases (pH = 7.0 ± 0.5). The <sup>13</sup>C longitudinal relaxation time constant (T<sub>1</sub>) of [2-<sup>13</sup>C]DHAc with PhGA was 35.2 ± 1.8 s at 7 T and 19.9 ± 1.0 s at 14.1 T. Radical quenching was confirmed by making seven frozen beads from the dissolved sample and averaging 100 ESR measurements to compensate for the dilution following dissolution. As confirmation, no ESR signal was observed.

**Table 2. DNP results obtained with 8 M [2-<sup>13</sup>C]DHAc samples polarized using a HyperSense polarizer with liquid-state polarizations measured 16 s after dissolution at 7 T.**

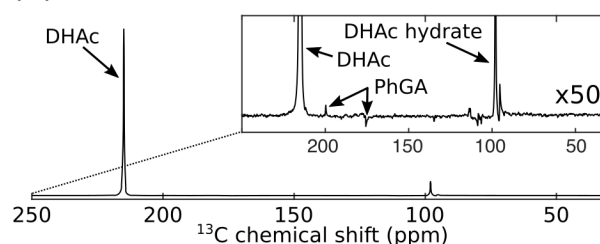
[2- <sup>13</sup> C] DHAc doped with	Build-up time constant (s)	Liquid-state <sup>13</sup> C polarization (%)
(1) PhGA	1033 ± 82	3.1 ± 0.8
(2) PhGA & Gd <sup>3+</sup>	1023 ± 97	5.1 ± 1.2
(3) d <sub>5</sub> -PhGA & Gd <sup>3+</sup>	862 ± 81	4.7 ± 1.0
(4) Trityl & Gd <sup>3+</sup>	1611 ± 353	16.0 ± 4.0

[2-<sup>13</sup>C]DHAc (213.9 ppm) and [2-<sup>13</sup>C]DHAc hydrate (96.6 ppm) dominated the hyperpolarized <sup>13</sup>C spectrum recorded in the 7 T MR scanner (Fig. 5a). The two peaks at 199.4 ppm and 175.3 ppm correspond to the resonances of [1-<sup>13</sup>C]PhGA and [2-<sup>13</sup>C]PhGA, respectively. No recombination products from the quenched radical were detected in the hyperpolarized <sup>13</sup>C spectrum.

A few impurities from the [2-<sup>13</sup>C]DHAc sample were observed at chemical shifts of 91.6 ppm, 94.9 ppm, 108.1 ppm, 105.9 ppm and 112.7 ppm. The same small quantities of impurities were also detected in the same solution before it had been UV-irradiated or polarized by DNP (Fig. 5b-iii). No additional peaks were detected in the thermally polarized spectra of the samples that had undergone photo-irradiation or photo-irradiation and subsequent DNP (Fig. 5b).

In comparison, a sample prepared with [2-<sup>13</sup>C]DHAc doped with 21 mM OX063 and 1.2 mM Gd<sup>3+</sup> polarized nearly 1.6 times slower than the samples with PhGA-derived radical but reached 3 times higher liquid-state polarization levels (Table 2). Interestingly, the T<sub>1</sub> at 7 T after dissolution of the [2-<sup>13</sup>C]DHAc sample with OX063 was 29.5 ± 0.5 s, ~5 s shorter than that of the sample with non-persistent PhGA-derived radical. It was also slightly shorter at 14.1 T, where the T<sub>1</sub> was 17.3 ± 1.4 s for [2-<sup>13</sup>C]DHAc with OX063. Note that the presence of 6 μM of Gd<sup>3+</sup> in the solution did not affect the T<sub>1</sub> of [2-<sup>13</sup>C]DHAc.

### (a) Hyperpolarized <sup>13</sup>C-MR at 7 T



### (b) Thermally-polarized <sup>13</sup>C-MR at 600 MHz

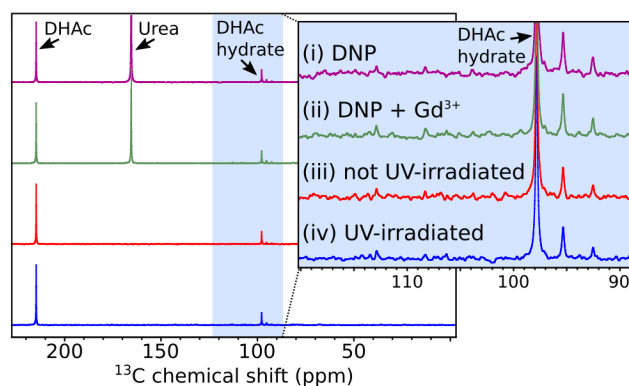


**Figure 5.** (a) Representative <sup>13</sup>C MR spectrum (sum of 180 spectra) of a hyperpolarized solution containing 40 mM [2-<sup>13</sup>C]DHAc, 5 mM PhGA and 6 μM Gd<sup>3+</sup> in PBS. The MR acquisition started 16 s after the beginning of the dissolution process with a repetition time = 1 s and nominal flip angle = 9°. (b) <sup>13</sup>C MR spectra of thermally-polarized solutions at 300 K and 14.1 T. All samples contained [2-<sup>13</sup>C]DHAc (40 mM-70 mM) and PhGA (4.5-8.0 mM) in PBS with 10% <sup>2</sup>H<sub>2</sub>O. [<sup>13</sup>C]urea was added to samples (i) and (ii) after dissolution as a reference. These samples were made from frozen beads of 8 M [2-<sup>13</sup>C]DHAc and 1 M PhGA in water. (i) Frozen beads had been irradiated using a narrowband light source (VisiCure 405 nm) for 200 s and dissolution DNP performed on them. (ii) 1.2 mM Gd<sup>3+</sup> had been added to the sample prior to photo-irradiation and dissolution DNP. (iii) The frozen beads were dissolved in PBS without photo-irradiation or DNP. (iv) The frozen beads were irradiated for 200 s and melted in PBS, but they did not undergo dissolution DNP.

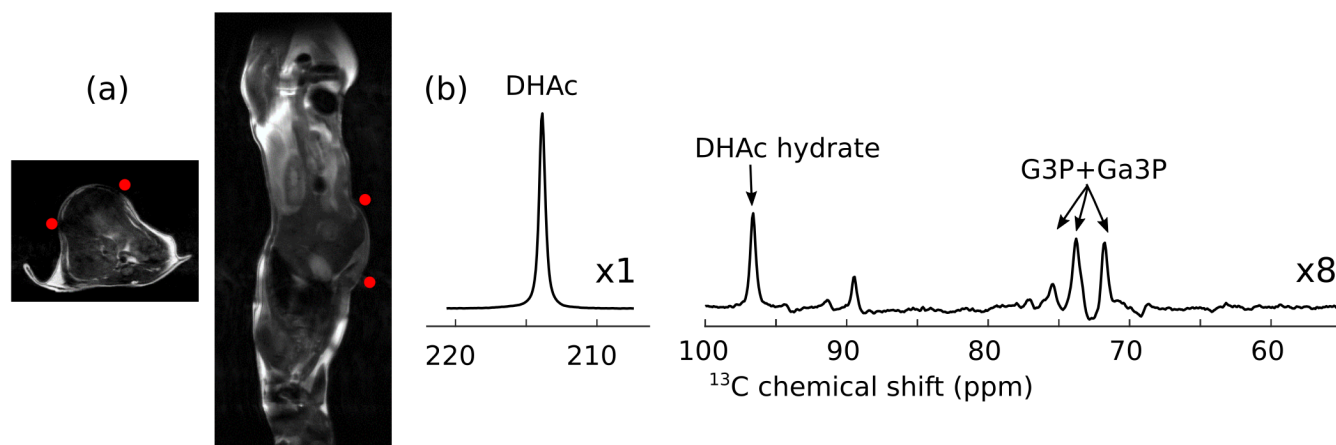


Figure 6. (a) Axial and sagittal  $T_2$ -weighted images through the mouse with approximate position of the surface coil (red dots represent the cross sections of the coil). (b)  $^{13}\text{C}$  MR spectrum acquired in vivo at 7 T following the intravenous injection of 400  $\mu\text{l}$  of a hyperpolarized solution into a mouse. The solution was composed of 40 mM  $[2\text{-}^{13}\text{C}]\text{DHAc}$ , 5 mM PhGA and 6  $\mu\text{M}$   $\text{Gd}^{3+}$  in PBS. The previously reported resonance detected at  $\sim 89$  ppm has not been assigned. DHAc region: sum of 40 spectra. Region with the metabolic products of DHAc and DHAc hydrate: sum of the first 70 spectra.

### In vivo $^{13}\text{C}$ MR of hyperpolarized $[2\text{-}^{13}\text{C}]\text{DHAc}$ metabolism

The  $^{13}\text{C}$  MR spectrum after the intravenous injection of 400  $\mu\text{l}$  of a hyperpolarized solution containing 40 mM  $[2\text{-}^{13}\text{C}]\text{DHAc}$ , 5 mM PhGA and 6  $\mu\text{M}$   $\text{Gd}^{3+}$  into a 32.2-g-mouse is shown in Figure 6. The injection of this solution did not cause any observable changes in the heart rate or respiratory pattern of the mouse. Since this sample was negatively polarized at 94.205 GHz, the  $^{13}\text{C}$  polarization was estimated to be 8.7% at the time of injection, which is 1.7 times higher than the  $^{13}\text{C}$  polarization recorded for the same sample positively polarized at 94.110 GHz (Table 2). Besides the injected DHAc and its hydrate, metabolic products were detected between 69 and 77 ppm. Note that the resonance appearing at  $\sim 89$  ppm has previously been reported in earlier in vivo studies,<sup>15</sup> but it has not been assigned. The peaks at 73.8 and 71.8 ppm could be seen for the first 20 s (first 90 acquisitions) and DHAc could be monitored for approximately 60 s (29 acquisitions). The  $T_1$  of  $[2\text{-}^{13}\text{C}]\text{DHAc}$  was determined to be  $15.8 \pm 0.3$  s in vivo.

## DISCUSSION

### PhGA as a radical precursor for DNP

Non-persistent radicals can be created through UV-Vis light irradiation of a precursor molecule. Although this is a simple procedure, the intense light used for the photo-generation of radicals may affect and degrade other molecules that are present in the sample. This is not the case for acetate or butyrate which can be used in conjunction with PA,<sup>12,13</sup> but some solvents (e.g. DMSO) and some metabolic substrates that are used with hyperpolarized  $^{13}\text{C}$  MR are photo-sensitive in the UV range. For example, most keto-acids - like PA - absorb light around 325 nm. DHAc, a metabolite that enters gluconeogenesis at the level of the trioses, has an absorption spectrum centered at 270 nm. We have shown that irradiation of DHAc and DMSO with a broadband UV-Vis source leads to the creation of radicals that are stable at 77 K. These radicals may not only affect the DNP process but also represent the unwanted degradation of these molecules. We have demonstrated that this degradation can be

avoided by using a narrowband light source in the visible spectrum in conjunction with PhGA as the radical precursor, which has an absorption spectrum that extends above 400 nm. The photochemistry of the radical generation upon photo-irradiation of PhGA and PA at 77 K are shown in Supplementary Figure 1.

A comparison between the efficiency of the two light sources in photo-generating radicals in PA and PhGA was made based on the wavelength-dependent power profile of each light sources and the absorption spectrum of the two precursors. This simple analysis assumes that radical generation is proportional to the density of photons absorbed by the precursors at each wavelength. Such comparison is only qualitative and most likely depends on many other factors such as light penetration and precursor concentration. Nevertheless, it reproduces the features observed experimentally, namely that while the broadband light source is more effective in PA radical photo-generation, the difference between the narrowband and the broadband light sources for PhGA radical photo-generation is relatively small, especially for samples containing  $\sim 1$  M precursor, which was the concentration used to polarize  $[2\text{-}^{13}\text{C}]\text{DHAc}$ .

The X-band ESR line width of photo-induced PhGA radicals is 1.4 mT, which is comparable to the line width of the OX063 trityl radical and much narrower than the photo-irradiated PA and TEMPOL line widths (see Sup. Fig. 4) – the latter nitroxyl radical having also previously been used to hyperpolarized  $^{13}\text{C}$ -substrates by dissolution DNP.<sup>21</sup> The four peaks observed in the ESR spectrum of PA (Fig. 2b) are due to coupling of the unpaired electron in C2 with the methyl group. The PhGA-derived radical exhibits a narrower line width than the PA-derived radical because the methyl group is substituted by a phenyl group, thereby increasing the distance between the unpaired electron localized around the ketone carbon and the neighboring protons, consequently reducing the hyperfine coupling. However, the non-negligible g-anisotropy of the photo-induced PhGA radical leads to a larger spread of the ESR absorption line compared to OX063, especially at the high fields where DNP is performed. Because narrow ESR line width radicals are generally more efficient for DNP,<sup>25</sup> especially at 3.35 T, PhGA was expected to be a competitive candidate for hyperpolarized  $^{13}\text{C}$  MR experiments using



the HyperSense polarizer. Although, the maximum  $^{13}\text{C}$  polarization obtained with photo-induction was lower than the one obtained with OX063, it was larger than what can typically be obtained with TEMPOL using the HyperSense.<sup>26,27</sup>

The  $\mu$ -wave spectrum acquired from samples polarized with photo-irradiated PhGA was nearly as narrow as that of the sample doped with OX063 but was clearly asymmetric because of the g-anisotropy of the PhGA-derived radical. Interestingly, no improvement in  $^{13}\text{C}$  polarization or significant change in  $\mu$ -wave spectrum (Sup. Fig. 3) could be detected using d<sub>5</sub>-PhGA, despite its 10% narrower ESR line width at X-band as compared to unlabeled PhGA. Again, this is most likely due to the non-negligible g-anisotropy of the PhGA-derived radical, which is exacerbated at 3.35 T as compared to X-band ESR measurements typically performed at 0.3 T.

At 3.35 T, the optimal concentration for OX063 trityl radical is 15–21 mM<sup>15,28</sup> and that of TEMPOL is 30–50 mM.<sup>29</sup> Hence, since the ESR line width of the PhGA-derived radical is only slightly broader than that of OX063, it was assumed that 15–25 mM of radical should be photo-generated in the PhGA samples in order to polarize  $^{13}\text{C}$ -enriched substrates using a HyperSense polarizer. This radical concentration can be achieved by irradiating 1 M PhGA for 150–200 s with a light source. Increasing the PhGA concentration in solution increased the photo-generated radical concentration up to 40 mM.

Previous studies showed that by adding  $\sim 1$  mM  $\text{Gd}^{3+}$  to a trityl-doped sample,  $^{13}\text{C}$  polarization could be greatly improved, possibly because  $\text{Gd}^{3+}$  causes a shortening in the  $T_1$  of the DNP-active electron spin in the low temperature regime.<sup>26,27</sup> We observed a similar trend in  $[2\text{-}^{13}\text{C}]\text{DHAc}$  samples prepared with PhGA-derived radical and doped with  $\text{Gd}^{3+}$ , with a nearly 2-fold increase in  $^{13}\text{C}$  liquid-state polarization.

The radical yield with photo-irradiated PhGA depended on pH. The highest radical yield was obtained when the solution containing the precursors was acidic, below the  $\text{pK}_a$  of PhGA ( $\text{pK}_a = 2.3$ ), and it decreased as pH was increased. A similar effect has been observed for UV-irradiated aqueous solutions of PA.<sup>30</sup> Therefore, PhGA is a radical precursor that is better adapted for acidic formulations of DNP samples. Conversely, TEMPOL cannot be used to polarize acidic samples because it spontaneously degrades.

PhGA has itself been shown to be an interesting probe for detecting hydrogen peroxide using hyperpolarized  $^{13}\text{C}$  MR.<sup>18</sup> The proposed method herein could obviously be used to hyperpolarize  $^{13}\text{C}$ -PhGA samples following photo-irradiation with visible light. The presence of a  $^{13}\text{C}$  spin on the ketone carbon will broaden the ESR spectrum through an additional hyperfine coupling and hence most likely reduce its efficiency for DNP at 3.35 T, but as already shown with  $^{13}\text{C}$ -PA this can be mitigated by increasing the magnetic field of the polarizer and using  $\mu$ -wave frequency modulation.<sup>27</sup>

#### Hyperpolarization of $[2\text{-}^{13}\text{C}]\text{DHAc}$ with PhGA-derived radical

The highest liquid-state  $^{13}\text{C}$  polarization – measured in a phantom 16 s after dissolution and obtained after having positively polarized a  $[2\text{-}^{13}\text{C}]\text{DHAc}$  sample containing photo-generated PhGA radical – was 5%. The estimated liquid-state  $^{13}\text{C}$  polarization in the sample negatively polarized that was injected in the mouse for in vivo application was 8.7% 16 s after dissolution. This is approximately 2 times lower than the maximum  $^{13}\text{C}$  polarization obtained with OX063 radical. In the framework of a potential clinical study, part of this difference could be recovered thanks to the fact that no filtration and quality control for residual radicals would be required, possibly allowing for a more rapid release of the dose for injection. In addition, because

they can be annihilated in the solid-state,<sup>11</sup> non-persistent photo-generated radicals can enable storage and transport, which would certainly benefit future clinical studies. It is also likely that the  $^{13}\text{C}$  polarization could be improved by performing DNP at higher magnetic fields and/or lower temperatures as well as by modulating the  $\mu$ -wave frequency, as was previously demonstrated with the photo-induced radical in PA.<sup>12,19,31</sup>

An additional advantage of photo-generated radicals is the longer lifetime of  $^{13}\text{C}$  hyperpolarization in liquid state. The  $^{13}\text{C}$   $T_1$  of  $[2\text{-}^{13}\text{C}]\text{DHAc}$  measured at 7 T and at 14.1 T immediately after dissolution was 15–20% longer in the solution prepared with PhGA than in the solution containing 0.1 mM OX063. This is a significant but not large change because the dominant relaxation mechanism at high magnetic fields is due to chemical shift anisotropy (CSA). However, at lower magnetic fields, such as in the stray magnetic field experienced by the solution during transfer between the polarizer and MR system, paramagnetic relaxation dominates<sup>32</sup> and the difference in  $T_1$  between the two types of solutions is expected to be much greater. Therefore, in a clinical setting where the transfer time is much longer and the solution might be located in a magnetic field as low as earth's magnetic field, quenching the radical will help maintain the  $^{13}\text{C}$  polarization until the solution is injected.<sup>33</sup> Removing paramagnetic relaxation of the hyperpolarized nuclei will also benefit other research fields that use dissolution DNP as a signal enhancement method, such as low field NMR or the study of long-lived singlet states.<sup>34,35</sup>

The impurities observed in the hyperpolarized  $^{13}\text{C}$  MR spectra of  $[2\text{-}^{13}\text{C}]\text{DHAc}$  were also observed in a thermally-polarized sample that had neither been photo-irradiated nor hyperpolarized. This shows that the molecule of interest stays intact during both the photo-irradiation and the dissolution DNP processes.

In analogy with what has been observed with photo-irradiated beads of frozen PA, the only expected recombination products of the PhGA-derived radical are  $\text{CO}_2$  and benzoic acid.<sup>10</sup> Electrospray ionization mass spectrometry analysis showed benzoic acid as the sole product of PhGA photo-irradiation (Sup. Fig. 5). This is further supported by the results of Lippert *et al.* who showed that, when reacted with hydrogen peroxide, the only product of hyperpolarized  $[2\text{-}^{13}\text{C}]\text{PhGA}$  is  $[1\text{-}^{13}\text{C}]\text{benzoic acid}$ .<sup>18</sup>

#### $^{13}\text{C}$ MR measurements of hyperpolarized $[2\text{-}^{13}\text{C}]\text{DHAc}$ metabolism in vivo

PhGA is a moderate acid ( $\text{pK}_a = 2.3$ ) with  $\text{LD}_{50} = 180$  mg/kg in mice,<sup>36</sup> and is excreted via urinary elimination.<sup>37</sup> In fact, a pharmacokinetic study where PhGA was injected intravenously into rats confirmed that PhGA did not metabolize and that it was excreted via urinary elimination within  $\sim 50$  min (apparent first-order rate of elimination of PhGA is  $\sim 0.1025\text{ min}^{-1}$ ).<sup>38</sup> The injection of 400  $\mu\text{l}$  of the hyperpolarized  $[2\text{-}^{13}\text{C}]\text{DHAc}$  solution (50 mM) containing 5 mM of PhGA ( $\sim \text{LD}_{50}/20$ ) into a 32-g mouse did not affect monitored physiological parameters. Nevertheless, daily exposure to large doses of PhGA (above 200 mg/kg) should be avoided because of potential neurotoxicity due to its amination product,  $\alpha$ -phenylglycine, which leads to depletion of striatal dopamine.<sup>39</sup> Less than 100  $\mu\text{M}$  of  $\text{CO}_2$  and benzoic acid were expected to be present in the solution following recombination of the PhGA-derived radical. The  $\text{CO}_2$  most likely escaped during the dissolution process and such a low concentration of benzoic acid is below the doses used therapeutically in humans.<sup>40</sup>

Many liver pathologies, such as non-alcoholic fatty-liver disease, are characterized by an aberrant glucose metabolism. Hyperpolarized [2-<sup>13</sup>C]DHAc – which follows gluconeogenesis, glycolysis and fatty acid synthesis – has been previously used to study hepatic metabolism. For example, the metabolic products of hyperpolarized [2-<sup>13</sup>C]DHAc in perfused mouse livers reported on differences between fed and fasted metabolic states.<sup>14</sup> Hepatic metabolic changes after a fructose injection were also detected in vivo using hyperpolarized [2-<sup>13</sup>C]DHAc.<sup>16</sup>

Here, the main metabolic product of hyperpolarized [2-<sup>13</sup>C]DHAc in the liver, glycerol 3-phosphate, was clearly seen in the <sup>13</sup>C MR spectrum as a doublet (75.7 and 71.8 ppm), with glyceraldehyde 3-phosphate in the middle at 73.8 ppm. Smaller peaks were also detected, which are probably metabolites of the gluconeogenic and glycolytic pathways, including lactate, glucose and glycerol, as reported in a <sup>1</sup>H-decoupled spectrum of perfused liver.<sup>14</sup> Although it has been observed in previous in vivo studies,<sup>16</sup> the [2-<sup>13</sup>C]phosphoenolpyruvate resonance (~152 ppm) was not observed in this experiment because it was outside the excitation bandwidth of the pulse used for radiofrequency excitation.

The <sup>13</sup>C T<sub>1</sub> of [2-<sup>13</sup>C]DHAc in vivo was ~16 s at 7 T. This is significantly shorter than the ~25 s previously reported in a 3 T MRI scanner,<sup>15</sup> supporting the conclusion derived from our phantom experiments that CSA is an important relaxation mechanism at high field. The apparent signal decay time constants of the metabolic products and DHAc hydrate were similar to that reported in rats in vivo.<sup>16</sup> The DHAc-to-metabolite ratio was ~70, which is about 2.5 times higher than that reported in perfused liver.<sup>14</sup> This is consistent with the fact that regions outside the liver contribute to the DHAc signal, while its metabolites are mainly produced in the liver. These data show that the method proposed herein can be used for metabolic studies of the liver in vivo.

## CONCLUSIONS

We have described a method to generate a photo-induced radical for dissolution DNP in samples containing photo-sensitive molecules. The method was used to hyperpolarize [2-<sup>13</sup>C]DHAc with the radical precursor PhGA using the commercial HyperSense polarizer. The non-persistent radical generated by photo-irradiation of PhGA was quenched after dissolution, increasing the <sup>13</sup>C longitudinal relaxation time. The liquid-state <sup>13</sup>C polarization was only half of the maximum polarization obtained with OX063 trityl radical but was nevertheless sufficient to report on the metabolism of the gluconeogenic and glycolytic probe [2-<sup>13</sup>C]DHAc in vivo. The <sup>13</sup>C polarization could be improved by using a higher field hyperpolarizer and optimizing the photo-generated radical concentration. Photo-irradiated PhGA could also become an attractive polarizing agent for the remote production of hyperpolarized <sup>13</sup>C-molecules since it was demonstrated that non-persistent photo-generated radicals can be annihilated in the solid state.<sup>11</sup>

## ASSOCIATED CONTENT

### Supporting Information

PDF containing supporting figures, mathematical description of the hyperpolarized signal corrected by flip angle and T<sub>1</sub> relaxation, and details on the perdeuteration of phenylglyoxylic acid.

Pg. S2:

Scheme 1. Radical production upon photo-irradiation of phenylglyoxylic acid and pyruvic acid at 77 K.

Mathematical description of the hyperpolarized signal corrected by flip angle and T<sub>1</sub> relaxation.

Pg. S3:

Supp. Fig. 1. ESR spectrometer calibration curve.

Pg. S4:

Supp. Fig. 2. Radical yield as a function of photo-irradiation time of PhGA, PA and DHAc.

Supp. Fig. 3. Solid-state microwave spectra of [2-<sup>13</sup>C]DHAc doped with unlabeled and perdeuterated PhGA.

Pg. S5:

Supp. Fig. 4. First derivative and absorption ESR spectra of solutions containing OX063, TEMPOL, photo-irradiated PhGA, or photo-irradiated PA.

Pg. S6:

Supp. Fig. 5. Electrospray ionization mass spectrometry analysis of the mixture after 2h of photoirradiation of PhGA.

Pgs. S6-S9:

Synthesis data for the synthesis of deuterated PhGA.

## AUTHOR INFORMATION

### Corresponding Author

\* Irene Marco-Rius; University of Cambridge, UK; irene.marco-rius@cruk.cam.ac.uk

### Author Contributions

All authors have given approval to the final version of the manuscript.

### Funding Sources

European Union's Horizon 2020 European Research Council (ERC Consolidator Grant) under grant agreement No 682574 (ASSIMILES), a Cancer Research UK Programme grant (17242) and by the CRUK-EPSRC Imaging Centre in Cambridge and Manchester (16465). FK and SP received founding from a Marie Curie ITN studentship under grant agreement No 642773 (EUROPOL). AC received funding from a Marie Skłodowska-Curie grant agreement no. 713683 (COFUNDfellows-DTU).

## ACKNOWLEDGMENT

The authors would like to thank Dr. De-en Hu, Dominik McIntyre and Madhu Basetti for technical help; Dr. Michael Tayler (University of Cambridge) and Mark Van Crielinge (University of California San Francisco) for fruitful discussions. This work is part of a project that has received funding from the European Union's Horizon 2020 European Research Council (ERC Consolidator Grant) under grant agreement No 682574 (ASSIMILES). FK and SP received founding from the European Union's Horizon 2020 research and innovation program under the Marie Skłodowska-Curie grant agreement No 642773 (EUROPOL). AC received funding from the European Union's Horizon 2020 research and innovation program under the Marie Skłodowska-Curie grant agreement no. 713683 (COFUNDfellowsDTU).

## ABBREVIATIONS

MR, magnetic resonance; PhGA, phenylglyoxylic acid; PA, pyruvic acid, DMSO, dimethyl sulfoxide; DHAc, dihydroxyacetone; G3P, glycerol 3-phosphate; LN<sub>2</sub>, liquid nitrogen; DNP, dynamic nuclear polarization; PBS, phosphate saline buffer;  $\mu$ -wave, microwave.

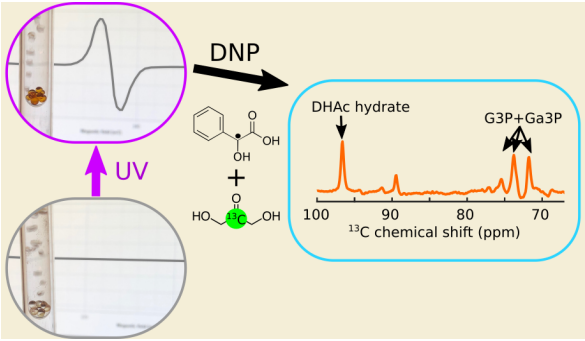
## REFERENCES

- Ardenkjaer-Larsen, J. H.; Fridlund, B.; Gram, A.; Hansson, G.; Hansson, L.; Lerche, M. H.; Servin, R.; Thanning, M.; Golman, K. Increase in Signal-to-Noise Ratio of >10,000 Times in Liquid-State NMR. *Proc Natl Acad Sci USA* **2003**, *100* (18), 10158–10163.

- (2) Lee, Y.; Heo, G. S.; Zeng, H.; Wooley, K. L.; Hilty, C. Detection of Living Anionic Species in Polymerization Reactions Using Hyperpolarized NMR. *J Am Chem Soc* **2013**, *135* (12), 4636–4639.
- (3) Marco-Rius, I.; Comment, A. In Vivo Hyperpolarized <sup>13</sup>C MRS and MRI Applications. In *Encyclopedia of Magnetic Resonance*; Harris, R. K., Wasylishen, R. L., Eds.; John Wiley & Sons, Ltd: Chichester, UK, 2018.
- (4) Lumata, L.; Ratnakar, S. J.; Jindal, A.; Merritt, M.; Comment, A.; Malloy, C.; Sherry, A. D.; Kovacs, Z. BDPA: An Efficient Polarizing Agent for Fast Dissolution Dynamic Nuclear Polarization NMR Spectroscopy. *Chem. Eur. J.* **2011**, *17* (39), 10825–10827.
- (5) Nelson, S. J.; Kurhanewicz, J.; Vigneron, D. B.; Larson, P. E. Z.; Harzstark, A. L.; Ferrone, M.; van Crielinge, M.; Chang, J. W.; Bok, R.; Park, I.; Reed, G.; Carvajal, L.; Small, E. J.; Munster, P.; Weinberg, V. K.; Ardenkjaer-Larsen, J. H.; Chen, A. P.; Hurd, R. E.; Odegardstuen, L.-I.; Robb, F. J.; Tropp, J.; Murray, J. A. Metabolic Imaging of Patients with Prostate Cancer Using Hyperpolarized [<sup>13</sup>C]Pyruvate. *Sci Transl Med* **2013**, *5* (198), 198ra108.
- (6) Brindle, K. M. Imaging Metabolism with Hyperpolarized <sup>13</sup>C-Labeled Cell Substrates. *J Am Chem Soc* **2015**, *137*, 6418–6427.
- (7) Kurhanewicz, J.; Vigneron, D. B.; Brindle, K.; Chekmenev, E. Y.; Comment, A.; Cunningham, C. H.; DeBerardinis, R. J.; Green, G. G.; Leach, M. O.; Rajan, S. S.; Rizi, R. R.; Ross, B. D.; Warren, W. S.; Malloy, C. R. Analysis of Cancer Metabolism by Imaging Hyperpolarized Nuclei: Prospects for Translation to Clinical Research. *Neoplasia* **2011**, *13* (2), 81–97.
- (8) Hyperpolarized [<sup>13</sup>C] Pyruvate Documentation Page | Cancer Imaging Program (CIP) [https://imaging.cancer.gov/programs\\_resources/cancer-tracer-synthesis-resources/hyperpolarized-C13-pyruvate-documentation.htm](https://imaging.cancer.gov/programs_resources/cancer-tracer-synthesis-resources/hyperpolarized-C13-pyruvate-documentation.htm) (accessed Oct 6, 2018).
- (9) Ardenkjaer-Larsen, J. H.; Leach, A. M.; Clarke, N.; Urbahn, J.; Anderson, D.; Skloss, T. W. Dynamic Nuclear Polarization Polarizer for Sterile Use Intent. *NMR Biomed* **2011**, *24* (8), 927–932.
- (10) Eichhorn, T. R.; Takado, Y.; Salameh, N.; Capozzi, A.; Cheng, T.; Hyacinthe, J. N.; Mishkovsky, M.; Roussel, C.; Comment, A. Hyperpolarization without Persistent Radicals for in Vivo Real-Time Metabolic Imaging. *Proc Natl Acad Sci USA* **2013**, *110* (45), 18064–18069.
- (11) Capozzi, A.; Cheng, T.; Boero, G.; Roussel, C.; Comment, A. Thermal Annihilation of Photo-Induced Radicals Following Dynamic Nuclear Polarization to Produce Transportable Frozen Hyperpolarized <sup>13</sup>C-Substrates. *Nat Commun* **2017**, *8*, 1–7.
- (12) Capozzi, A.; Hyacinthe, J. N.; Cheng, T.; Eichhorn, T. R.; Boero, G.; Roussel, C.; Van Der Klink, J. J.; Comment, A. Photoinduced Nonpersistent Radicals as Polarizing Agents for X-Nuclei Dissolution Dynamic Nuclear Polarization. *J Phys Chem C* **2015**, *119* (39), 22632–22639.
- (13) Bastiaansen, J. A. M.; Yoshihara, H. A. I.; Capozzi, A.; Schwitter, J.; Gruetter, R.; Merritt, M. E.; Comment, A. Probing Cardiac Metabolism by Hyperpolarized <sup>13</sup>C MR Using an Exclusively Endogenous Substrate Mixture and Photo-Induced Nonpersistent Radicals. *Magn Reson Med* **2018**, *79* (5), 2451–2459.
- (14) Moreno, K. X.; Satapati, S.; DeBerardinis, R. J.; Burgess, S. C.; Malloy, C. R.; Merritt, M. E. Real-Time Detection of Hepatic Gluconeogenic and Glycogenolytic States Using Hyperpolarized [2-<sup>13</sup>C]Dihydroxyacetone. *J Biol Chem* **2014**, *289*, 35859–35867.
- (15) Marco-Rius, I.; Cao, P.; von Morze, C.; Merritt, M.; Moreno, K. X.; Chang, G.-Y.; Ohliger, M. A.; Pearce, D.; Kurhanewicz, J.; Larson, P. E. Z.; Vigneron, D. B. Multiband Spectral-Spatial RF Excitation for Hyperpolarized [2-<sup>13</sup>C]Dihydroxyacetone <sup>13</sup>C-MR Metabolism Studies. *Magn Reson Med* **2017**, *77* (4), 1419–1428.
- (16) Marco-Rius, I.; von Morze, C.; Sriram, R.; Cao, P.; Chang, G.-Y.; Milshteyn, E.; Bok, R. A.; Ohliger, M. A.; Pearce, D.; Kurhanewicz, J.; Larson, P. E. Z.; Vigneron, D. B.; Merritt, M. Monitoring Acute Metabolic Changes in the Liver and Kidneys Induced by Fructose and Glucose Using Hyperpolarized [2-<sup>13</sup>C]Dihydroxyacetone. *Magn Reson Med* **2017**, *77* (1), 65–73.
- (17) European Commission, D.-G. for H. and C. *Opinion on Dihydroxyacetone*; 2010.
- (18) Lippert, A. R.; Keshari, K. R.; Kurhanewicz, J.; Chang, C. J. A Hydrogen Peroxide-Responsive Hyperpolarized <sup>13</sup>C MRI Contrast Agent. *J Am Chem Soc* **2011**, *133* (11), 3776–3779.
- (19) Capozzi, A.; Karlsson, M.; Petersen, J. R.; Lerche, M. H.; Ardenkjaer-Larsen, J. H. Liquid-State <sup>13</sup>C Polarization of 30% through Photo-Induced Non-Persistent Radicals. *J Phys Chem C* **2018**, *122* (13), 7432–7443.
- (20) Heraeus. SUPRASIL 1, 2, 3 and SUPRASIL Standard <http://www.unitedlens.com/pdf/suprasil.pdf> (accessed Jul 10, 2018).
- (21) Comment, A. Dissolution DNP for in Vivo Preclinical Studies. *J Magn Reson* **2016**, *264*, 39–48.
- (22) Rodrigues, T. B.; Serrao, E. M.; Kennedy, B. W. C.; Hu, D.-E.; Kettunen, M. I.; Brindle, K. M. Magnetic Resonance Imaging of Tumor Glycolysis Using Hyperpolarized <sup>13</sup>C-Labeled Glucose. *Nat Med* **2014**, *20* (1), 93–97.
- (23) Mishkovsky, M.; Anderson, B.; Karlsson, M.; Lerche, M. H.; Sherry, A. D.; Gruetter, R.; Kovacs, Z.; Comment, A. Measuring Glucose Cerebral Metabolism in the Healthy Mouse Using Hyperpolarized <sup>13</sup>C Magnetic Resonance. *Sci Rep* **2017**, *7* (1), 4–11.
- (24) Rapf, R. J.; Perkins, R. J.; Carpenter, B. K.; Vaida, V. Mechanistic Description of Photochemical Oligomer Formation from Aqueous Pyruvic Acid. *J Phys Chem A* **2017**, *121* (22), 4272–4282.
- (25) Comment, A.; Merritt, M. E. Hyperpolarized Magnetic Resonance as a Sensitive Detector of Metabolic Function. *Biochem.* **2014**, *53* (47), 7333–7357.
- (26) Ardenkjaer-Larsen, J. H.; Macholl, S.; Johannesson, H. Dynamic Nuclear Polarization with Triyls at 1.2 K. *Appl. Magn. Reson.* **2008**, *34*, 509–522.
- (27) Lumata, L.; Merritt, M. E.; Malloy, C. R.; Sherry, A. D.; Kovacs, Z. Impact of Gd3+ on DNP of [1-<sup>13</sup>C]Pyruvate Doped with Trityl OX063, BDPA, or 4-Oxo-TEMPO. *J. Phys. Chem. A* **2012**, *116* (21), 5129–5138.
- (28) Wolber, J.; Ellner, F.; Fridlund, B.; Gram, A.; Jóhannesson, H.; Hansson, G.; Hansson, L. H.; Lerche, M. H.; Månsson, S.; Servin, R.; Thaning, M.; Golman, K.; Ardenkjaer-Larsen, J. H. Generating Highly Polarized Nuclear Spins in Solution Using Dynamic Nuclear Polarization. *Nucl Instrum Meth A* **2004**, *526*, 173–181.
- (29) Comment, A.; van den Brandt, B.; Uffmann, K.; Kurdziesau, F.; Jannin, S.; Konter, J. A.; Hautle, P.; Wenckeback, W. T.; Gruetter, R.; van der Klink, J. J. Design and Performance of a DNP Prepolarizer Coupled to a Rodent MRI Scanner. *Concepts Magn Reson B* **2007**, *31* (4), 255–269.
- (30) Rapf, R. J.; Dooley, M. R.; Kappes, K.; Perkins, R. J.; Vaida, V. PH Dependence of the Aqueous Photochemistry of α-Keto Acids. *J Phys Chem A* **2017**, *121* (44), 8368–8379.
- (31) Cheng, T.; Capozzi, A.; Takado, Y.; Balzan, R.; Comment, A. Over 35% Liquid-State <sup>13</sup>C Polarization Obtained via Dissolution Dynamic Nuclear Polarization at 7 T and 1 K Using Ubiquitous Nitroxyl Radicals. *Phys Chem Phys* **2013**, *15* (48), 20819.
- (32) Cheng, T.; Mishkovsky, M.; Bastiaansen, J. A.; Ouari, O.; Hautle, P.; Tordo, P.; van den Brandt, B.; Comment, A. Automated Transfer and Injection of Hyperpolarized Molecules with Polarization Measurement Prior to in Vivo NMR. *NMR Biomed.* **2013**, *26*, 1582–1588.
- (33) Comment, A. The Benefits of Not Using Exogenous Substances to Prepare Substrates for Hyperpolarized MRI. *Imaging Med* **2014**, *6* (1), 1–3.
- (34) Tayler, M. C. D.; Levitt, M. H. Paramagnetic Relaxation of Nuclear Singlet States. *Phys Chem Chem Phys* **2011**, *13* (20), 9128–9130.
- (35) Marco-Rius, I.; Tayler, M. C. D.; Kettunen, M. I.; Larkin, T. J.; Timm, K. N.; Serrao, E. M.; Rodrigues, T. B.; Pileio, G.; Ardenkjaer-Larsen, J. H.; Levitt, M. H.; Brindle, K. M. Hyperpolarized Singlet Lifetimes of Pyruvate in Human Blood and in the Mouse. *NMR Biomed.* **2013**, *26* (12), 1696–1704.
- (36) Sigma-Aldrich. Phenylglyoxylic acid <https://www.sigmaaldrich.com/MSDS/MSDS/DisplayMSDSPage.do?country=GB&language=en&productNumber=B13055&brand=ALDRICH&PageToGoToURL=https%3A%2F%2Fwww.sigmaaldrich.com%2Fcatalog%2Fproduct%2Faldrich%2Fb13055%3Flang%3Den> (accessed Jul 9, 2018).
- (37) Guillemin, M. P.; Bauer, D. Human Exposure to Styrene III. Elimination Kinetics of Urinary Mandelic and Phenylglyoxylic Acids after Single Experimental Exposure. *Int Arch Occup Env. Heal.* **1979**,

- 44, 249–263.
- (38) Amin, Y. M.; Nagwekar, J. B. Utilization of Model Compounds to Evaluate Effects of Slight Chemical Modifications on Their Distribution Pharmacokinetic Parameters in Rats and Mechanisms Inferred for Their Transmembrane Transport. *J. Pharm. Sci.* **1975**, *64* (11), 1804–1812.
- (39) Terre'blanche, G.; Heyer, N.; Jacobus, •; Bergh, J.; Lodewyk, •; Mienie, J.; Cornelius, •; Van Der Schyf, J.; Harvey, B. H. The Styrene Metabolite, Phenylglyoxylic Acid, Induces Striatal-Motor Toxicity in the Rat: Influence of Dose Escalation/Reduction over Time. *Neurotox. Res.* **2011**, *20*, 97–101.
- (40) Batshaw, M. L.; MacArthur, R. B.; Tuchman, M. Alternative Pathway Therapy for Urea Cycle Disorders: Twenty Years Later. *J. Pediatr.* **2001**, *138*, S46–S55.

Table of Contents artwork





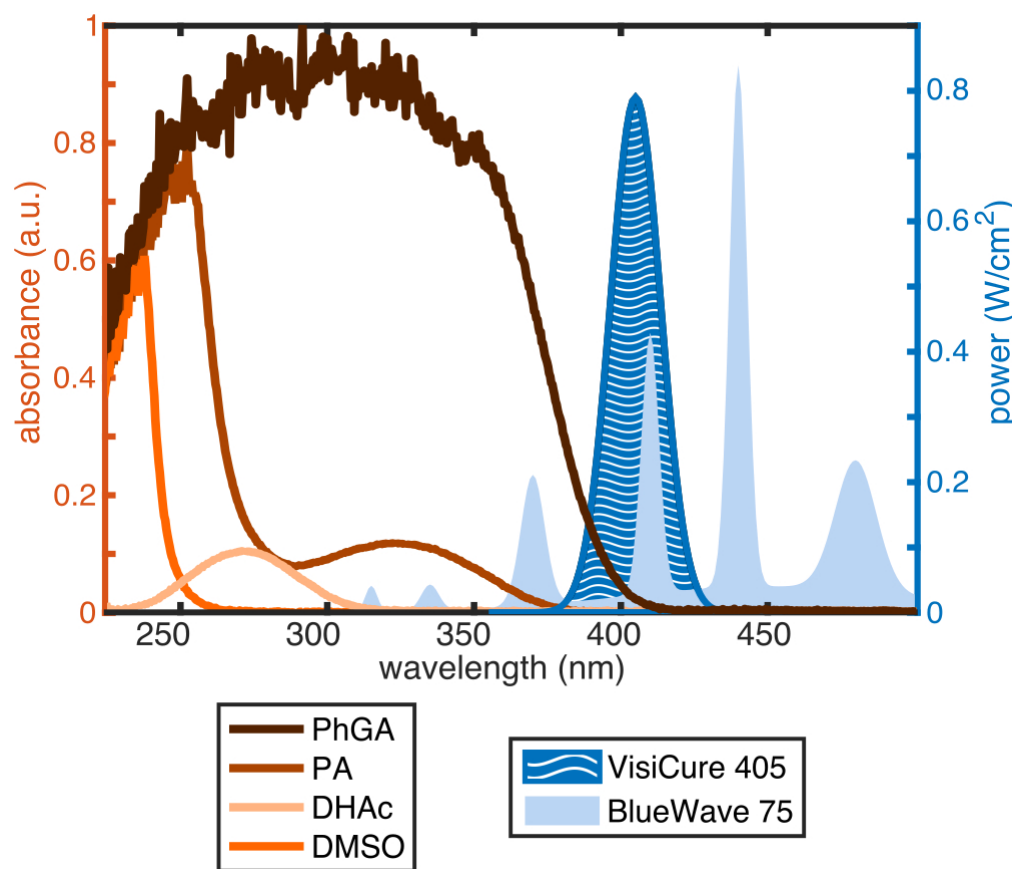


Figure 1. UV-Vis absorption spectra (left axis) and light source power distributions (right axis). Power profiles were provided by the manufacturer (Dymax Europe GmbH, Wiesbaden, Germany).

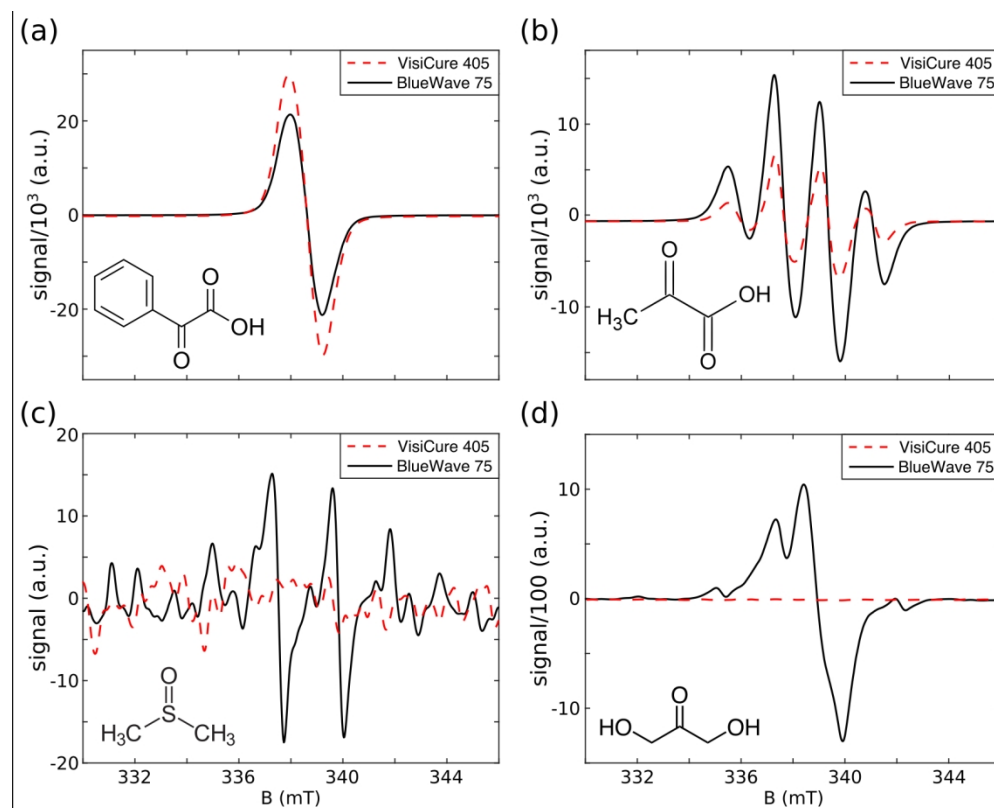


Figure 2. X-band ESR spectra of frozen droplets in LN<sub>2</sub>, photo-irradiated with a broadband (BlueWave 75) or a narrowband (VisiCure 405) light source. (a) PhGA (7.1 M) in 1:1 water/glycerol (v/v). (b) PA (7.0 M) in 1:1 water/glycerol (v/v). (c) DMSO (neat). (d) DHAc (8.0 M) in <sup>2</sup>H<sub>2</sub>O. The spectral structure in (b) and (c) are caused by the hyperfine coupling to the proton spins of the methyl groups. The units on the y-axis are the same in all four plots.

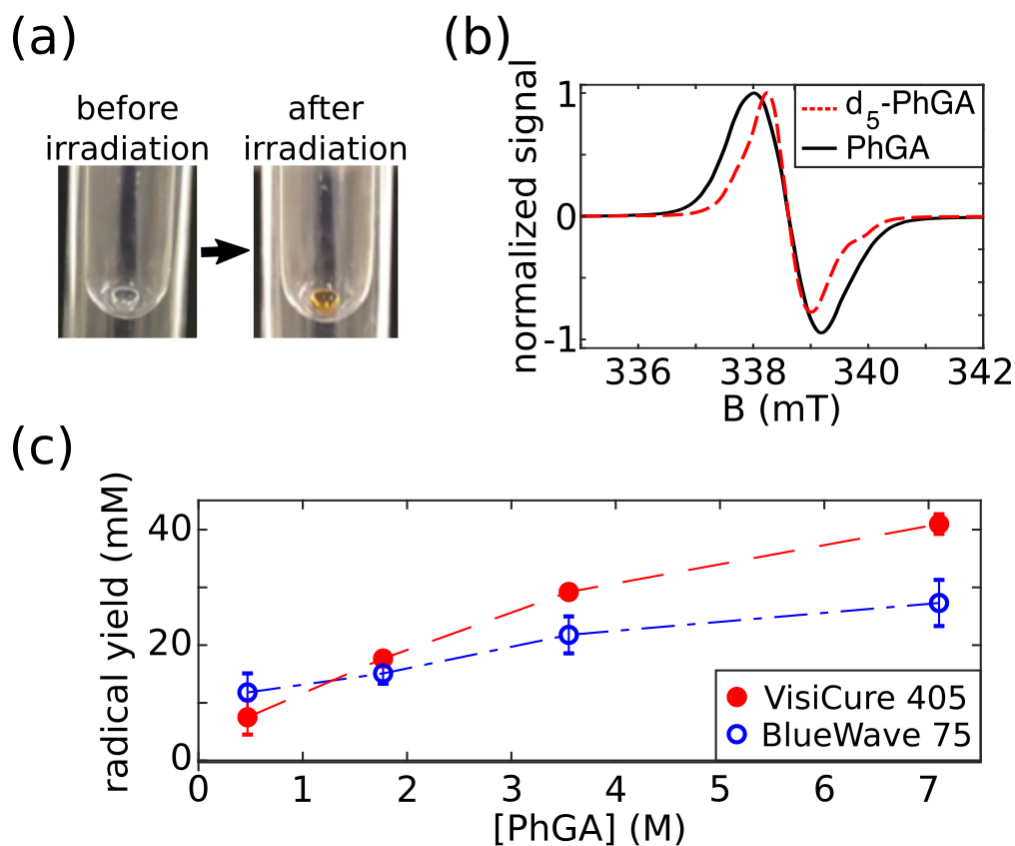


Figure 3. Photo-irradiation of PhGA dissolved in 1:1 glycerol/water (v/v). (a) 4- $\mu$ l-bead of PhGA in  $LN_2$  before and after photo-irradiation. (b) ESR spectrum of unlabeled PhGA and  $d_5$ -PhGA. (c) Maximum radical yield vs. PhGA concentration using either the broadband (blue open circle) or the narrowband light source (red dots). Radical yield is reported as mean  $\pm$  standard deviation across 3 measurements.

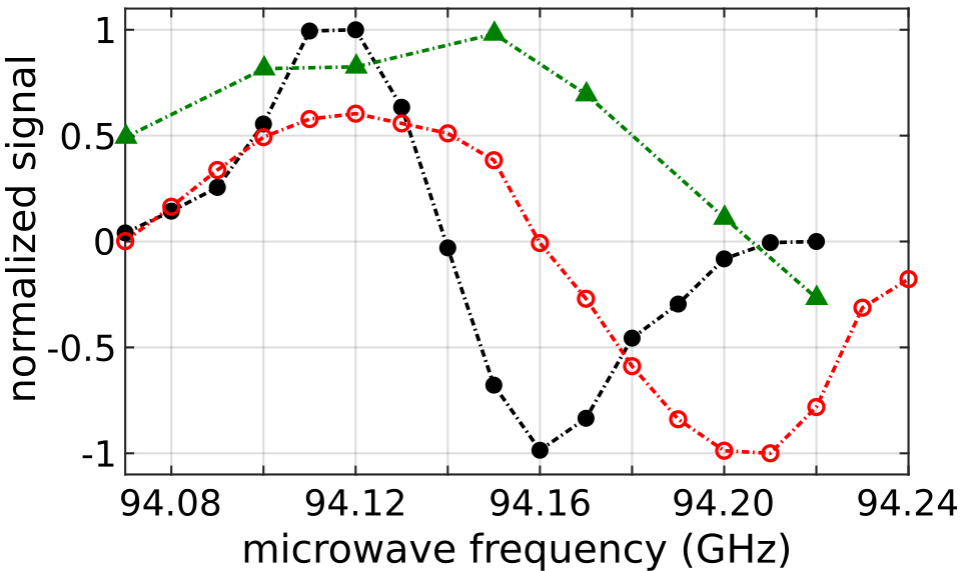


Figure 4. Solid-state microwave spectra at 3.35 T and 1.25 K: (red open circles) photo-irradiated [2-<sup>13</sup>C]DHAc solution (8 M) in H<sub>2</sub>O doped with 1 M PhGA (18 mM radical); (black dots) [2-<sup>13</sup>C]DHAc solution (8 M) in H<sub>2</sub>O/DMSO (v/v) doped with 21 mM OX063; (green triangles) photo-irradiated [1-<sup>13</sup>C]PA solution (7 M) in H<sub>2</sub>O/glycerol (65 mM radical).

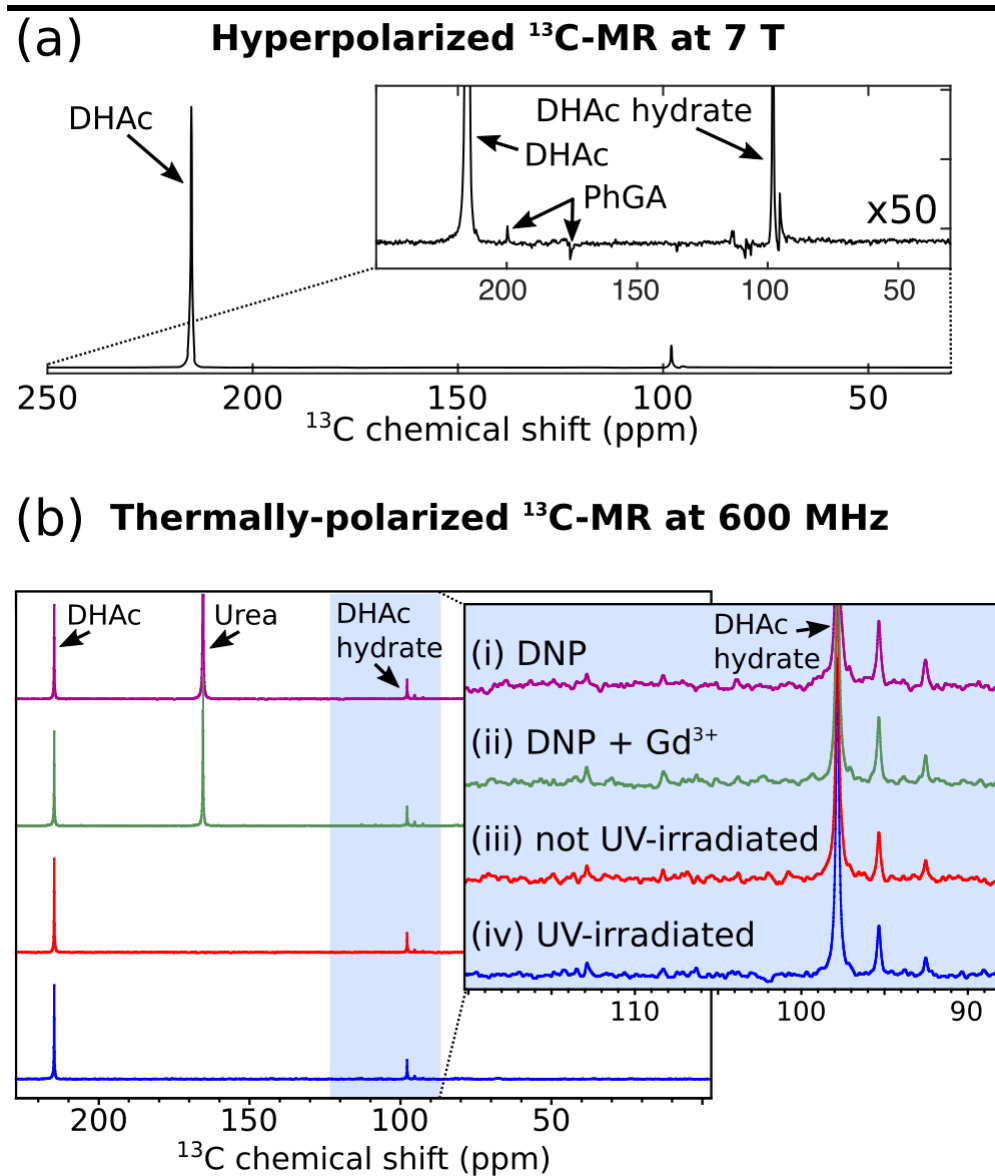


Figure 5. (a) Representative  $^{13}\text{C}$  MR spectrum (sum of 180 spectra) of a hyperpolarized solution containing 40 mM  $[2\text{-}^{13}\text{C}]\text{DHAc}$ , 5 mM PhGA and  $6\text{ }\mu\text{M}$   $\text{Gd}^{3+}$  in PBS. The MR acquisition started 16 s after the beginning of the dissolution process with a repetition time = 1 s and nominal flip angle =  $9^\circ$ . (b)  $^{13}\text{C}$  MR spectra of thermally-polarized solutions at 300 K and 14.1 T. All samples contained  $[2\text{-}^{13}\text{C}]\text{DHAc}$  (40 mM-70 mM) and PhGA (4.5-8.0 mM) in PBS with 10%  $^2\text{H}_2\text{O}$ .  $[^{13}\text{C}]\text{urea}$  was added to samples (i) and (ii) after dissolution as a reference. These samples were made from frozen beads of 8 M  $[2\text{-}^{13}\text{C}]\text{DHAc}$  and 1 M PhGA in water. (i) Frozen beads had been irradiated using a narrowband light source (VisiCure 405 nm) for 200 s and dissolution DNP performed on them. (ii) 1.2 mM  $\text{Gd}^{3+}$  had been added to the sample prior to photo-irradiation and dissolution DNP. (iii) The frozen beads were dissolved in PBS without photo-irradiation or DNP. (iv) The frozen beads were irradiated for 200 s and melted in PBS, but they did not undergo dissolution DNP.



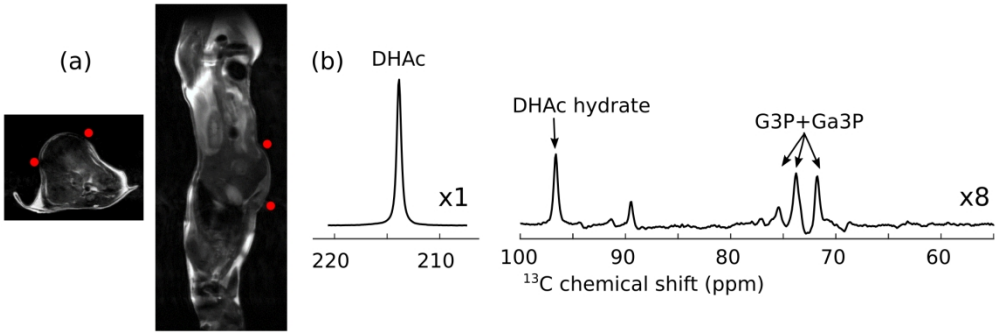


Figure 6. (a) Axial and sagittal  $T_2$ -weighted images through the mouse with approximate position of the surface coil (red dots represent the cross sections of the coil). (b)  $^{13}\text{C}$  MR spectrum acquired in vivo at 7 T following the intravenous injection of 400  $\mu\text{l}$  of a hyperpolarized solution into a mouse. The solution was composed of 40 mM  $[2\text{-}^{13}\text{C}]\text{DHAc}$ , 5 mM PhGA and 6  $\mu\text{M}$   $\text{Gd}^{3+}$  in PBS. The previously reported resonance detected at  $\sim 89$  ppm has not been assigned. DHAc region: sum of 40 spectra. Region with the metabolic products of DHAc and DHAc hydrate: sum of the first 70 spectra.